Construction of a diode-pumped 532 nm Nd:YVO_4 laser with Cr:YAG passive *Q*-switching and intracavity KTP frequency doubling

Aaron J. Lemmer
Univ. of Wisconsin-River Falls, Physics Dept.
River Falls, WI 54022

A laser-diode end-pumped Nd:YVO_4 laser with passive *Q*-switching and intracavity frequency doubling is presented. The frequency doubling is accomplished by implementing a KTP nonlinear crystal in the resonator, while the passive *Q*-switching is attempted using a Cr:YAG saturable absorber. An actively *Q*-switched system is realized, and a minimum pulse width of 477 ± 32 ns and a peak-power-to-cw-power ratio of 12.28 ± 0.50 were obtained at a repetition rate of 3.921 ± 0.020 kHz with an incident 808 nm pump beam having an output power of 602.0 ± 1.6 mW. In addition to these measurements, for a pump power of 970 ± 20 mW, the continuous-wave output of the laser is shown to have a stability better than ±0.038 % over a time period longer than one hour.

I. INTRODUCTION

Diode-pumped solid-state lasers with intracavity passive *Q*-switching and frequency doubling have recently proven to be well-suited for small- and medium-power applications in both industry and academia, owing to efficient and cost-effective designs as well as reliable performance. Neodymium lasers with second-harmonic generation can offer additional practical advantages such as single-frequency visible light output and minimal power source and thermal control requirements. Collectively, the development of these solid-state lasers has benefited fields spanning medicine (e.g. cosmetic surgery, urology), holography (e.g. data storage, interferometry), and materials processing. Laser-diode-pumped, Nd-doped solid-state lasers with either intracavity frequency doubling or passive *Q*-switching are not new in concept, having been presented or analyzed in numerous publications.[1] Due to recent exploration of Cr:YAG saturable absorbers as an intracavity passive *Q*-switch, reports on diode-pumped green lasers with both intracavity frequency doubling and passive *Q*-switching have earned increased interest.[2]

A laser-diode-pumped 532 nm Nd-doped yttrium otrthovanadate (YVO_4) laser with both intracavity KTP frequency doubling and Cr:YAG passive *Q*-switching is presented in this paper. According to Zheng *et al*., the advantages of Cr:YAG as a saturable absorber for passive *Q*-switching include its large excited-state absorption cross section, capacity for high doped-ion

concentration, high damage threshold, good thermal conductivity, and its stable physical, thermal, and photochemical properties.[3] The laser presented herein realizes stable green TEM_{00} operation with the Nd:YVO_4 and KTP crystals and then the saturable absorber is inserted to attain *Q*-switched output; the laser is then characterized, considering such parameters as average power, pulse width, peak power, repetition rate, and pump power.

I.A. Laser Fundamentals

'Laser' is an acronym that stands for 'light amplification by the stimulated emission of radiation.' To fully comprehend the laser design presented in this paper, a basic understanding of the radiative processes which can occur between populations of electrons in two energy levels (namely, absorption and stimulated emission), the requirements for producing and maintaining a balance of these processes, and the techniques exploited to amplify or modify their effects is essential.

I.A.1. Detailed Balance and Stimulated Emission

The light emitted by a laser is a result of energy transfer between two distinct energy levels in the laser medium via radiation. The ratio of the population densities N_u and N_l (the number of particles per unit volume) of atoms with electrons inhabiting the upper and lower energy levels E_u and E_l, respectively, can be expressed in terms of Boltzmann statistics as:

$$\frac{N_u}{N_l} \propto e^{-\Delta E_{ul}/k_b T} \tag{1}$$

where $\Delta E_{ul} = E_u - E_l$ and k_b is Boltzmann's constant, and the assumption that $E_u > E_l$ is asserted.[4]

Several processes can influence the ratio defined by Equation 1. Natural radiative decay, also known as spontaneous emission, occurs in all excited-state systems but it is not necessarily probabilistically favored. In solids, interactions with surrounding atoms (phonons) or with photons can stimulate the depopulation or excitation of energy levels. Stimulated absorption—or

just absorption—is a well-known phenomenon by which an input of electromagnetic energy, in the form light, can 'stimulate' an electron into a higher energy state. The notion that the reverse process—the stimulated emission (or decay) of an excited electron by an impingent photon—is also possible is an interpretation of the principle of detailed balance that is attributed to Albert Einstein. By this principle, in equilibrium two conditions are satisfied: firstly, the influx of particles to a given quantum state per unit time is balanced by the number of particles exiting that state per unit time when in equilibrium and, second, the number of particles entering that state via a specific conduit—say, a stimulated process—is balanced by the number of particles leaving that state by the same means.[5] Mathematically, this principle is dictated by the radiative thermal equilibrium constraint:

$$N_u A_{ul} + N_u B_{ul} u(\nu) = N_l B_{lu} u(\nu) \tag{2}$$

where $u(\nu)$ is the photon energy density (energy per unit volume-frequency), A_{ul} is the spontaneous emission probability (a rate of decay per unit time), B_{lu} and B_{ul} are the stimulated proportionality constants such that the upward and downward fluxes (number of stimulated transitions per unit volume per unit time per unit frequency) are given by the second and third terms in Equation 2.[6]

Collectively, the three constants A_{ul}, B_{ul}, and B_{lu} are dubbed the Einstein A and B coefficients, and it can be shown that they are related as follows:[7]

$$B_{ul} = \frac{c^3}{8\pi h \eta^3 \nu^3} A_{ul} = \frac{g_l}{g_u} B_{lu} \cong B_{lu} \tag{3}$$

where c is the speed of light, h is Planck's constant, η is the index of refraction, ν is the frequency corresponding to the energy level separation, and where the statistical weight factors (g) can be simplified as $g_l \approx g_u$ for solid-state laser media.

The three abovementioned radiative events—spontaneous emission, absorption, and stimulated emission—are illustrated by Figure 1.[8] Three characteristic properties of laser beams are direct results of these processes. For stimulated absorption to occur, the photon impingent on the lower-level electron must have an energy $E = hv$ such that it exactly matches the separation between the energy levels. Likewise, the energy of the incident photon must be equal to the energy level separation in order for an electron to be released by stimulated emission; when this happens, by the laws of conservation of energy and momentum, an additional photon is emitted with identical energy, propagation direction, and phase as that incident photon.[9]

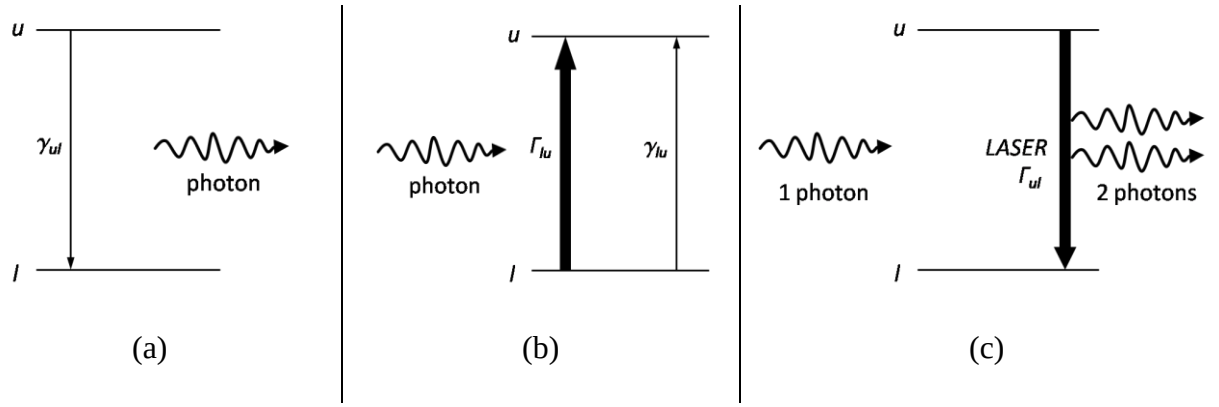

Figure 1: Dominant radiative transitions between energy levels u and l ($E_u > E_l$) in a laser are shown. (a) Spontaneous emission. (b) Absorption. (c) Stimulated emission. See text for further explanation.

I.A.2. Requirements for Light Amplification (Gain) in Solid-State Laser Media

The intensity (as a power per unit cross-sectional area) of a light beam as it propagates through a length z of solid-state laser gain medium, can be directly derived from Equations 1-3:

$$I(z) = I_0 e^{\sigma_{ul}(N_u - N_l)z} \tag{4}$$

where I_0 is the intensity of the beam prior to entering the gain medium, $I(z)$ is the intensity of the beam after penetrating a distance z into the medium, and the value σ_{ul}—called the stimulated emission cross section—has units of length^2 and is essentially constant for a particular laser level transition in a specific laser gain medium.[10]

As is apparent from Equation 4, the intensity of the light beam will be amplified as long as the population density of the upper laser level N_u remains larger than the population density of the lower laser level N_l. This is not a normal equilibrium condition, and thus it is appropriately termed a population inversion. Maintaining this population inversion is essential to the maintaining stimulated emission: if the population density in the lower level is smaller than in the upper level, then less electrons are available for stimulated absorption when photons with energy equal to ΔE_{ul} impinge upon the system, and therefore stimulated emission becomes the favored stimulated radiative process.

Equation 4 also implies that, as long as a population inversion is maintained, the intensity of the beam will increase exponentially with linearly increasing length of the laser gain medium. In reality, this exponential growth is limited by several factors. A gain medium with finite cross-sectional dimensions and linearly increasing length (i.e., a gain medium with a finite population of atoms available for laser transitions) cannot meet the exponential growth demands of the laser beam, so conceivably there is a depth or length z into the medium at which the intensity saturates and begins to grow linearly. This length is called the saturation length L_{sat} and the intensity at which saturation occurs is given by:

$$I_{sat} = \frac{h\nu_{ul}}{\sigma_{ul}(\nu)\tau_u} \tag{5}$$

where ν_{ul} is the frequency corresponding to the laser level separation and τ_u is the lifetime of the upper laser level.[11]

I.A3. Maintenance of a Stable Laser

Lasers with gain media much longer than the saturation length are not always practical—they offer little in the way of increased intensity as compensation for the difficulties presented in aligning them. Instead of increasing the physical dimensions of the gain medium (e.g. using a

larger crystal), highly-reflective mirrors can be introduced at both ends of the crystal to form a cavity that increases its effective length. This configuration in essence creates an infinite chain of images of the crystal behind the mirrors, because the light can oscillate back and forth through the medium until the gain is adequate to reach the saturation intensity, and also attains a very low-divergence beam.[12] In order to allow light to be emitted from the cavity, one of the mirrors—the output coupler—is designed to have a lower reflectivity, allowing some laser light to be transmitted. By forming a cavity, laser light is permitted to oscillate internally sufficiently many times to amplify and balance the radiative rates for stabilized laser output.

Again, the most important requirement for a laser is that its population inversion be maintained; as previously stated, this implies that more electrons be available for stimulated emission than for absorption. One way to accomplish this is to continuously excite the electrons in the lower level—by a process known as pumping. An ideal laser system is diagrammed in Figure 2, and it has four distinct energy levels: the lowest level, *0*; the lower laser level, *l*; the upper laser level, *u*; and the highest level, *i*; where $0 < l < u < i$. The pump inputs a photon with energy equivalent to $\Delta E_{0i} = E_i - E_0$ and thus excites electrons from level *0* to level *i* (at a rate of Γ_{0i}); from level *i*, the dominant transition is spontaneous—and most likely collisional—decay to *u* occurring at a rate of γ_{iu}. Due to the large energy separation with respect to ΔE_{0i}, spontaneous decay from *i* to *l* or to *0* is possible, but not probable. From level *u*, the spontaneous decay at rate γ_{ul} can trigger photons of an energy suited for triggering a cascade of stimulated laser emission. Due to the large amount of photons with energy E_{ul} passing through the gain medium, dominating stimulated emission, and population inversion, transitions from *l* to *u* and *u* to *0* are not likely. Level *l* is populated largely through laser emission, and depopulated through

spontaneous decay at a rate γ_{l0}, which is a rapid transition on account of an ideally small energy difference between levels *l* and *0*.

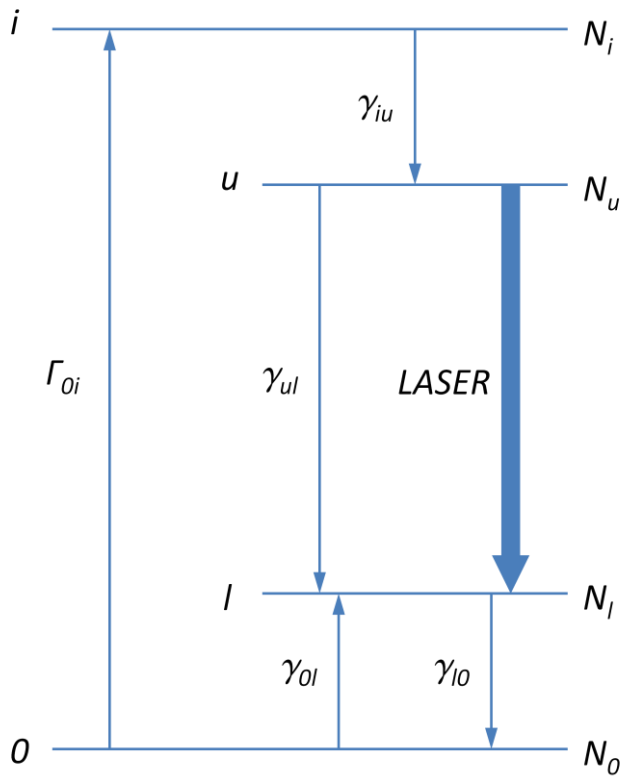

Figure 2: A four-level laser system is shown, illustrating the dominant radiative transitions. The upper and lower laser levels are designated as *u* and *l*, with energies $E_u > E_l$ and population densities N_u and N_l, respectively. Levels *i* and *0* are above *u* and below *l*, respectively, with energies $E_i > E_u$ and $E_l > E_0$ and population densities N_i and N_0. The pump rate is designated as Γ_{0i}, the spontaneous transitions are designated by γ.

I.A4. Properties of a Two-Mirror Laser Resonator

The use of mirrors at the ends of the cavity was previously introduced as a method to increase the effective amplification length of the gain medium. This modification in effect makes the cavity a Fabry-Perot resonator, and introduces both frequency-dependent (longitudinal) and also spatial-dependent (transverse) electromagnetic effects that are diffraction-related.[13] Because the mirrors impose boundary conditions on the electromagnetic radiation—the laser beam—traveling between the mirrors, standing waves form via interference at a regular frequency spacing, as given by Equation 6:

$$\Delta \nu_{separation} = \frac{nc}{2}\left(\frac{1}{\eta_C (d-L) + \eta_L L}\right) \tag{6}$$

where $\Delta\nu_{separation}$ is the frequency spacing between interference intensity maxima, c is the speed of light, η_C is the index of refraction of the cavity medium, η_L and L are the index of refraction and length of the laser gain medium, and $n = 0, 1, 2, \ldots$ designates the mode number, or integer multiplicity of standing-wave frequencies that can form within a cavity of length d (note that n can be infinitely large).[14]

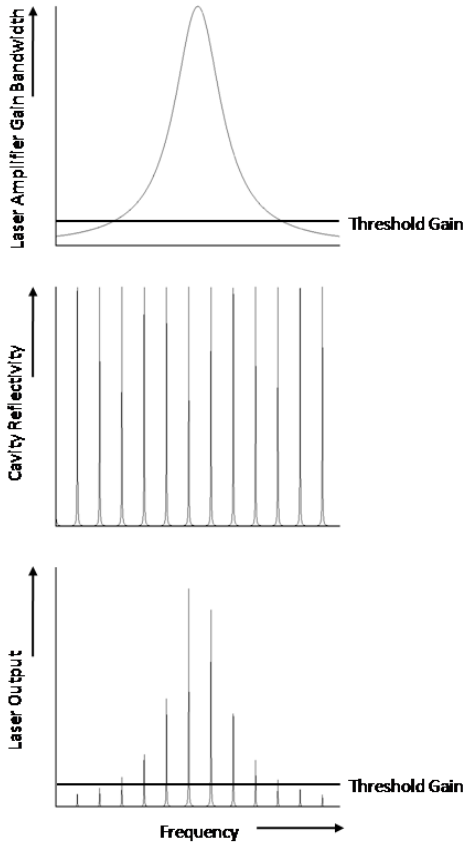

Figure 3: Longitudinal cavity modes in laser emission. (Top) The gain bandwidth is given as a function of emission frequency; the threshold gain (or, the level at which the gain exceeds losses in the cavity) is indicated with the horizontal line. (Middle) The reflectivity of the cavity is shown as a function of the frequency of light in the cavity. Sharp peaks occur at each resonant frequency. (Bottom) The intensity of the resulting laser cavity modes are displayed as a function of the frequency of laser output. The gain bandwidth is essentially a limiting 'envelope' on the maximum intensity at each resonant frequency. Note how only those frequencies which exceed the threshold gain are actually present in the laser output.[15]

The separation d of the mirrors institutes an optical path length difference and a phase change in the electromagnetic waves is introduced by the reflections, causing the interference. The frequencies corresponding to interference maximums are actually resonant frequencies resulting from the Fabry-Perot cavity, and these are collectively referred to as the longitudinal laser cavity modes. Because the cavity has a particular set of resonances, the laser emission bandwidth is enhanced at those resonant frequencies. Laser emission occurs at the resonant frequencies as long as the threshold gain is exceeded (as long as the amplification by stimulated emission exceeds any losses in the cavity), as is shown in Figure 3 above.[16]

The two-mirror resonator design also introduces transverse (spatial-dependent) laser cavity modes. Since the electromagnetic waves in the resonator are not plane waves of infinite lateral extent, the beam diffracts as it interacts with the components in the cavity.[17] These diffraction-loss-related effects, which are manifest in the transverse direction as visible patterns in the intensity profile of the beam, can be supported as steady-state modes because the laser amplifying medium still produces gain after it compensates for theses losses as well as loss due to mirror transmission, radiative absorption, and scattering.[18] To have a steady-state spatial mode, the spatial pattern of the beam profile's amplitude cannot change; i.e., the (x-y) amplitudes of the wave function $\psi'(x', y')$ that reflects off the cavity mirror M' must be proportional to the wave function $\psi(x, y)$ that reflects back toward M' from the other cavity mirror M for every point (x', y') on M'. This notion, visualized in Figure 4, can be described mathematically using an adaptation of the Fresnel-Kirchhoff Diffraction integral formula:

$$\psi'(x', y') = \gamma\psi(x', y') = C\iint_A \psi(x, y)e^{ik_1(xx'+yy')}dxdy \tag{7}$$

where C and k_1 are constants, the primes merely indicate the mirror or wave function being

considered, x and y are the coordinates in the transverse direction, γ is a proportionality constant that accounts for diffraction losses in the formation of the transverse modes (γ is unrelated to the γ describing spontaneous radiative transitions, but is consistent with original diffraction theory), and where the double integral is evaluated for light passing through an aperture A (such as the laser gain medium).

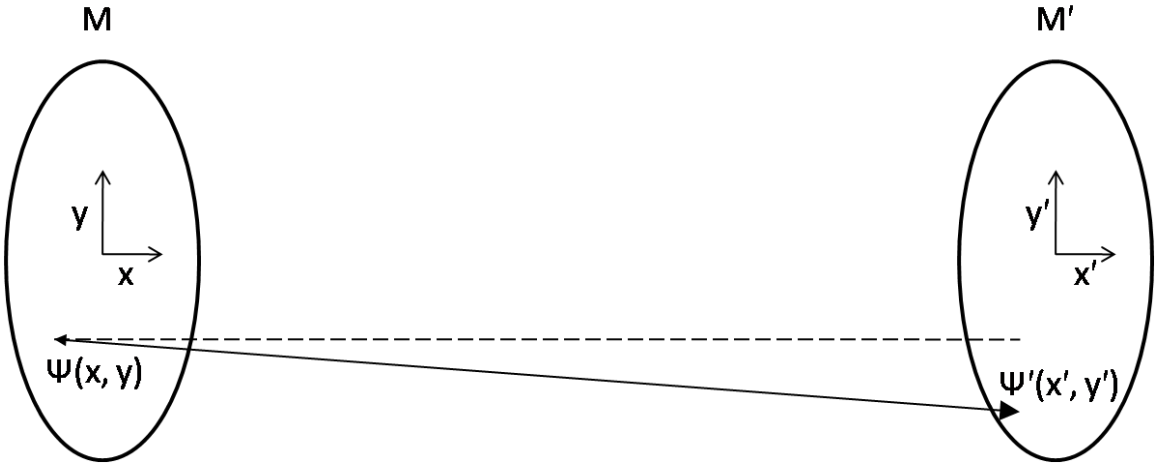

Figure 4: Parallel circular mirrors M and M' are illustrated with their respective x-y coordinate systems. For every source point (x', y') on the mirror M', the wave function $\psi(x, y)$ that reflects off M toward M' must be proportional to the wave function $\psi'(x', y')$ reflected back from M' to M with respect to the transverse amplitude pattern in order for a steady-state transverse mode to form. In other words, if the $\psi(x, y)$ propagating toward M' hypothetically has a transverse shape of a circle, then the $\psi'(x', y')$ returned from M' to M must be have a proportionally-sized transverse circle shape (as opposed to, for example, a distorted square shape).[19]

Mathematically it is quite clear that $\psi(x, y)$ is its own Fourier transform; i.e., the Fourier transform of $\psi(x, y)$ is $\psi(x', y')$ and vice versa.[20] $\Psi_{pq}(x, y)$, given in Equation 8, represents the most general solution to Equation 7 that satisfies this Fourier transform condition.[21] This set of wave function solutions is mathematically similar to that for a one-dimensional quantum harmonic oscillator.[22] Infinitely many forms of Equation 8 exist, corresponding to the each of the longitudinal mode numbers $n = 0, 1, 2, ...$, as given in Equation 6.

$$\psi_{pq}(x', y') = H_p\left(\frac{\sqrt{2}x}{w}\right) H_q\left(\frac{\sqrt{2}y}{w}\right) e^{-(x^2+y^2)/w^2} \tag{8}$$

where H_p and H_q are Hermite polynomials of orders p and q, respectively, and w is a constant. The Hermite polynomials are defined in Equation 9.

$$H_m(u) = (-1)^m e^{u^2} \frac{d^m}{du^m} e^{-u^2} \tag{9}$$

where m denotes the order of the Hermite polynomial and u is the argument of H_m.[23]

The transverse mode wave functions as given by Equation 8 are often termed TEM_{pq}, where TEM means 'transverse electromagnetic;' the TEM_{00} mode is just the Gaussian distribution. The physical representations of these TEM mode distributions are shown below in Figure 8.

I.B. Second Harmonic Generation

The laser system discussed below utilizes neodymium as the laser species, with a fundamental or natural laser emission wavelength of 1064.3 nm, which is infrared. Since this wavelength is invisible, a technique called second harmonic generation is employed to 'frequency double' the 1064 nm light to visible 532 nm (recall that frequency is inversely proportional to wavelength; i.e., when the frequency is doubled, the wavelength is halved). This technique exploits nonlinear optical effects in an anisotropic crystal to virtually 'sum' the frequencies ω of two identical incident photons; the two photons are destroyed, but simultaneously a single photon with a frequency of 2ω and identical propagation direction is generated.[24] An additional method called phase matching is utilized to maximize the frequency-doubling effect.[25]

I.C. *Q*-Switching

A technique called *Q*-switching can be used to generate short pulses of laser output, which are distinguished by peak powers and pulse energies that can be multiple orders of magnitude greater than the same laser in steady-state continuous wave operation. Consider a laser cavity which initially has very high cavity losses (high enough that the saturation intensity I_{sat} cannot be reached and oscillation between the mirrors cannot occur). Because the losses in the cavity are this great, the pump beam is granted an opportunity to increase the upper laser level population density N_u—and thus the population inversion—to a greater extent than in a system with a steady-state net gain. If this high cavity loss condition is then suddenly removed, the beam can then quickly form and extract this increased quantity of stored energy from the upper level in the form of a giant pulse (or 'surge') of stimulated emission. The method is dubbed *Q*-switching because, in rapidly changing the cavity loss from high to low, the cavity is switched from a low-*Q* state to a high-*Q* state. This *Q* is a quality factor, essentially the ratio of energy stored in the cavity to the energy dissipated inside the cavity; thus, the high cavity loss situation is a low-*Q* state, because the energy stored in the resonator is very low compared to the amount of energy being dissipated by the high-loss element in the cavity. The low cavity loss situation is conversely a high-*Q* state because much more energy can be stored in the resonator than is dissipated. In order for the population inversion to increase as described while the cavity losses are high, the lifetime τ_u of the upper laser level and the duration of pumping must be sufficiently long periods of time that the upper level can store excess energy pumped into it during that interval.

Q-switching depends upon the ability to rapidly change the cavity losses in the laser; this is like inserting a dam into a river and removing it in rapid succession, allowing the volume of

water to alternately build up behind the dam and then surge free. Several active methods effectively accomplish this requirement, including the use of a mechanical shutter to physically block and unblock the beam, a rotating cavity mirror to temporarily destabilize the cavity, or an electro-optic crystal (such as a Pockels cell or Kerr cell) and a polarizer to modulate the amplitude of the beam.[26] A saturable absorber—e.g. a Cr:YAG crystal—can be implemented into the laser cavity to act as a passive *Q*-switch.[27] Cr:YAG actually behaves as a laser medium if pumped at the fundamental Nd laser frequency (1064 nm), and is naturally highly-absorptive at 1064 nm until it reaches some saturation intensity, at which point the transmission of the crystal at 1064 nm increases and it becomes low-loss.[28]

II. EXPERIMENTAL PROCEDURE

II.A. Elements of the Experimental Setup

Figure 5 exhibits a schematic diagram for a *Q*-switched frequency-doubled Nd:YVO_4 laser in which a plane-concave cavity serves as the laser resonator. This configuration is stable for cavity lengths of $0 < l \leq r_{CM}$—where l is the length and r_{CM} is the radius of curvature of the concave mirror, a condition which allows the cavity to be arbitrarily compact (limited only by the sizes of the intracavity components). Narrower pulse widths (and therefore higher peak power) can be obtained by minimizing cavity length, hence the reasoning for choosing a plane-concave resonator.[29] Here the cavity is 120 ± 2 mm in length. The high reflector (HR) is a 12.5-mm-diameter plane mirror with antireflective (AR) coatings at 808 nm—the pump wavelength—on both the entrance face (R < 0.2%) and on the intracavity face (R < 5%).[30] The intracavity face of the HR is also coated for high-reflection at both the Nd^{3+} lasing wavelength of 1064 nm (R > 99.8%) and the frequency-doubled wavelength (R > 99% at 532 nm). The output coupler (OC) is a plano-concave mirror with a 12.5-mm diameter and a 200 mm radius of curvature.[31] The concave surface is coated for high-reflection at 1064 nm (R > 99.8%) and is

AR-coated at 532 nm (R < 5%), while the planar surface has just an AR coating for 532 nm (R < 0.2%).

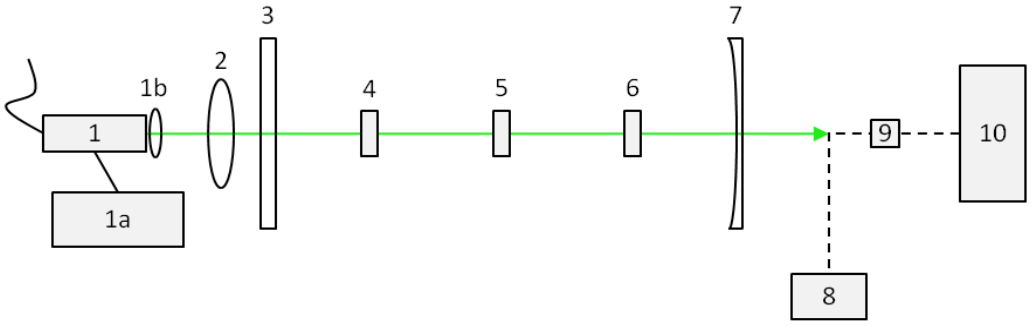

Figure 5: A schematic diagram for the end-pumped, *Q*-switched, frequency-doubled Nd:YVO_4 laser is shown, including data acquisition apparatus. (1) Fiber-coupled GaAs pump laser. (1a) Thermoelectric PID temperature control (TEC) for the pump laser. (1b) Small lens at end of fiber emitter used to collimate the pump beam. (2) 25-mm-focal-length lens used to focus the collimated pump beam into the Nd:YVO_4 crystal. (3) High reflector. (4) Nd^{3+}:YVO_4 gain medium. (5) *Q*-switching element. (6) KTP nonlinear frequency-doubling crystal. (7) Output coupler. (8) Power meter for cw measurements. (9) PIN photodiode for pulsed-wave power measurements. (10) Oscilloscope. The propagation of the laser is shown by the arrow.

A GaAlAs quantum-well laser diode (LD) with maximum power of 0.75 W, spectral width (FWHM) of <5 nm, and a typical divergence of 0.15 NA at 90% power serves as the pump source, and is fiber-coupled to the optical train in an end-pumping configuration.[32] The peak emission wavelength is tuned to the Nd:YVO_4 absorption peak at 808.9 ± 5.0 nm (at 25 °C) to maximize the pumping efficiency. A high-stability driver provides the current to operate the LD and a thermoelectric PID temperature controller (TEC) is implemented to steady the output power of the pump source, which in turn aids in stabilizing the power of the 532 nm output.[33] Since the cone divergence angle of the pump beam from the fiber coupler (about 16°) is large relative to the thickness of the Nd:YVO_4 crystal along the longitudinal axis of the beam, a pair of lenses are placed between the LD and HR (one of which is attached to the fiber coupler as shown in Figure 5) to collimate the pump beam and focus it onto the gain medium, thereby minimizing loss of pumping power.[34] The position of the lens relative to the LD, HR, and gain medium can

be adjusted by trial and error during the initial alignment process to optimize the pump efficiency (i.e., to maximize the average cw 532 nm output power).

A 2.95x3.05x1.0 mm^3 a-cut Nd:YVO_4 crystal doped with 1 at. % of Nd^{3+} ions serves as the gain medium of the laser.[35] As oriented in Figure 5, both the left and right facets of the Nd:YVO_4 crystal are AR-coated at the fundamental laser wavelength of 1064 nm (R < 0.1%) and the left facet is AR-coated at the 808-nm pump wavelength (R < 5%). Frequency doubling is accomplished in the laser with a KTP crystal (3x3 mm^2 in cross-section and 5 mm thick, type II noncritical phase matching).[36] Both surfaces of the KTP are AR-coated at 1064 nm and 532 nm (R <0.1% and R <0.5%, respectively). A Cr^{4+}:YAG saturable absorber (3x3 mm^2 in cross-section and 1 mm thick) with a small-signal 1064-nm transmission of T_0 = 85 % is employed to obtain passive *Q*-switching of the 532 nm output.[37] Both facets of the Cr:YAG crystal are polished and do not have AR coatings. Each of the three crystals is wrapped in indium-tin foil and set in a copper block (see Figure 6), which acts as a heat sink.

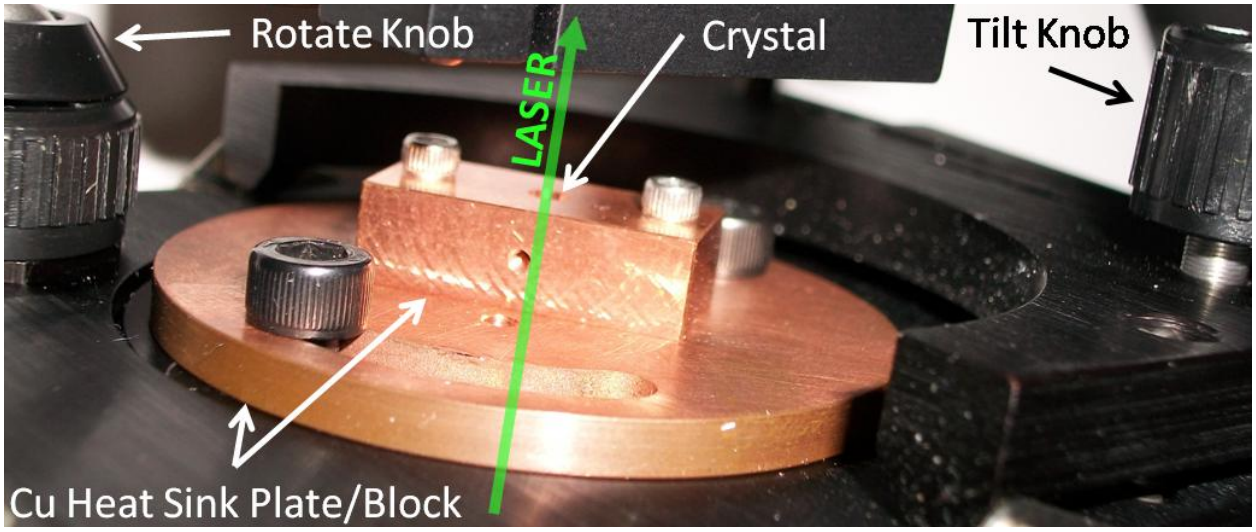

Figure 6: Each of the three crystals was mounted in copper heat-sinking blocks as illustrated. First, a crystal was wrapped in a thin layer of indium-tin foil, seated in a small circular recess in the copper block such that the foil acted as a thermal contact between the crystal and block, and then secured with a small set screw.

II.B. Construction and Alignment Procedure

Figure 7 is a photograph of the final construction of the laser. All components are mounted upon a small 2”-thick optical breadboard base and assembled at one end of a 10-foot optical table. A small HeNe alignment laser was secured to the other end of this table, leveled with respect to the table’s surface, and aimed parallel to its long edge and toward the breadboard.[38] The first component installed on the breadboard base was the HR cavity mirror, which was situated in a Gimbal mount and positioned at an arbitrary point along the optical path. [39] Gimbal mounts advantageously provide the capability of both pan and tilt fine-tuning about an object’s geometric center such that these adjustments not also translate the center (simplifying the alignment process). The HR was placed by first centering it vertically and horizontally on the HeNe beam and then, using the Gimbal controls on the mount, directing the reflected HeNe light back into the output aperture of the alignment laser.

The Nd:YVO_4 was then positioned about 7 mm to the right of the HR (see Figure 7). As mentioned above and as shown in Figure 6, the crystal was mounted in a copper heat-sink block; this block (and the similarly-mounted KTP crystal) was then attached to a circular copper plate which was subsequently fixed to a Gimbal optical mount also capable of rotating 360°.[40] The Nd: YVO_4 crystal, in its final mount, was placed on an optical post and centered on the alignment beam. The Gimbal controls were then used to direct the light reflected off the face of the gain medium back into the aperture of the HeNe laser. At this juncture, the frequency-doubling crystal (KTP) was placed inside the cavity and aligned using similar methods as the Nd:YVO_4. The cavity was then completed by adding the OC, which was mounted aligned in the same way as the HR; after this step was completed, the light at the output of the HeNe laser was

flickering. This observed behavior results from longitudinal interference of the alignment laser since the HR and OC essentially form a Fabry-Perot cavity (see Section I.A4).

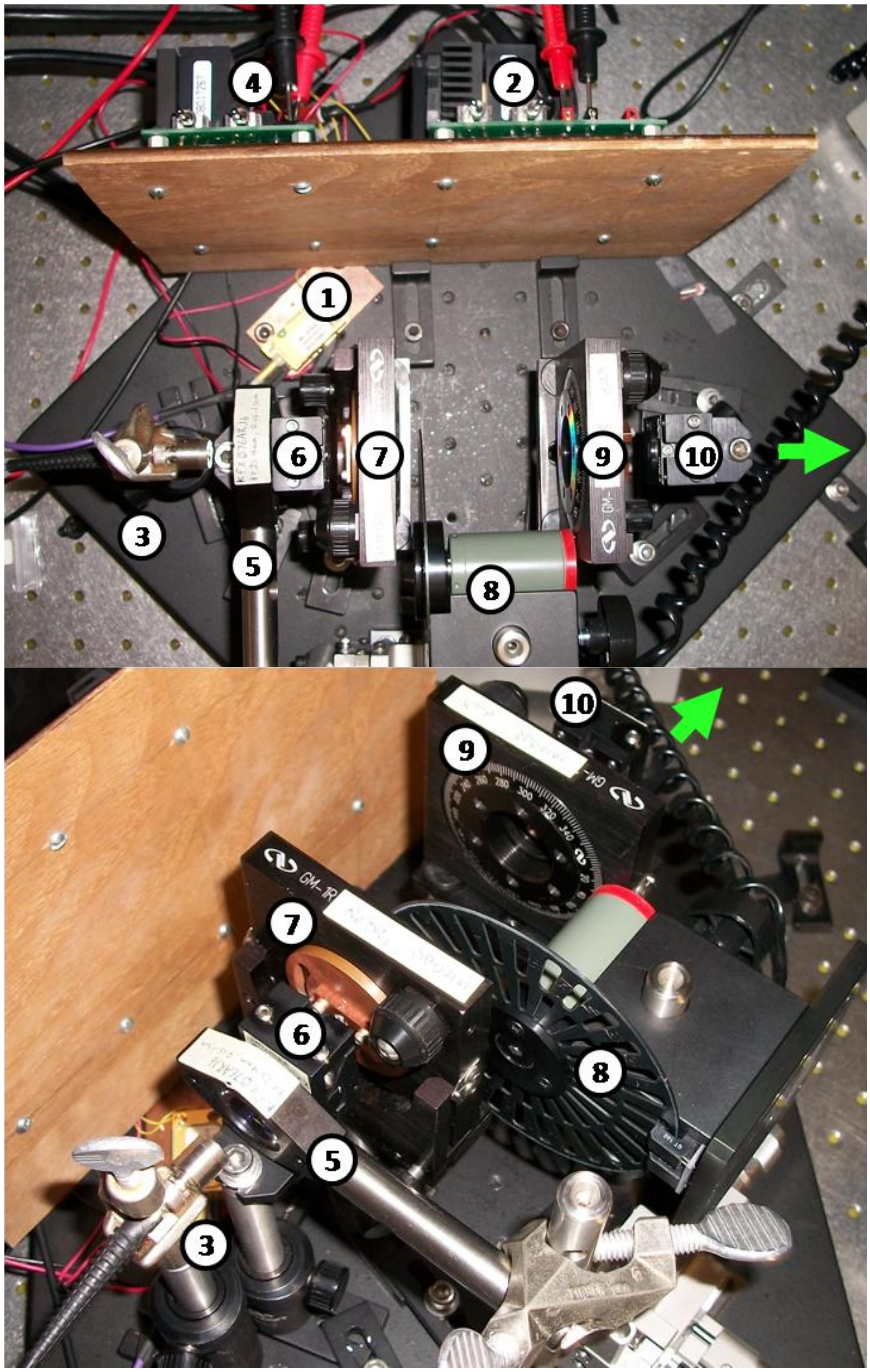

Figure 7: A photograph of the finished laser with pertinent components labeled. (1) GaAs LD. (2) LD Driver. (3) Fiber Coupler and Pump beam collimating lens. (4) TEC. (5) Pump beam focusing lens. (6) HR. (7) Nd^{3+}:YVO_4. (8) *Q*-switch. (9) KTP. (10) OC. The direction of propagation of the laser is indicated by the green arrow.

The pump laser assembly was then installed on the breadboard; the LD was secured to a small copper block which functions as a heat sink and was then clamped to the base as shown in Figure 3. The fiber coupler (comprised of an optical fiber and small attached coupling lens) was positioned in the path of the alignment laser approximately 24 mm to the left of the HR and adjusted until the front surface of the coupling lens reflected the alignment beam back into its output aperture. The secondary lens was then placed on a small XYZ translation stage in front of the output coupler at a distance of <3 mm such that the diverging pump beam did not overfill the lens (this was verified by direct observation; i.e., because the 808 nm beam is near-infrared, it can be seen to the naked eye at a sufficiently high power). This lens was roughly centered in the transverse directions on the alignment beam and then tilted until it redirected the HeNe beam back into the alignment laser output aperture.

After this initial alignment was finished, the LD was turned on and the tilt of the HR and OC were tweaked until green emission was achieved. The power was maximized by adjusting the *x*, *y*, and *z* positions of the focused pump beam on the Nd:YVO_4 crystal with the translation stage. To obtain pulsed output, the mounted Cr:YAG crystal was placed into the cavity between the KTP crystal and OC (the block containing the Cr:YAG crystal was fastened to an optical mount capable of 360° rotation in the transverse plane[41]) at the Brewster angle, and then aligned using the same HeNe procedure as for the other crystals.

II.C. Data Collection Setup and Procedure

The laser was characterized at two points during the construction process: after obtaining green cw output and after establishing pulsed output. Once green laser output was initially achieved, the cavity mirrors and crystal orientations were adjusted to obtain the TEM_{00} mode and to maximize the average output power. The cw power was measured for this step with a power

meter calibrated for 532 nm light.[42] Before attempting to attain pulsed output, the cw output power was sampled from the power meter at a rate of 2.5 GHz over an approximately one-hour-long time interval to determine the average cw power and the long-term output stability at a set pump power of 970±20 mW. After obtaining a pulsed beam the *Q*-switched output was characterized for several pumping powers, considering important parameters including the average output power, pulse width, peak power, and repetition rate; these were determined using the statistics and measurement modules of a digital oscilloscope and then plotted as functions of pump power.[43] A PIN photodiode was utilized in order to make measurements of the pulsed beam, since the power meter attenuator was not rated to withstand the high peak power of the pulses.[44]

III. ANALYTICAL PROCEDURE AND DISCUSSION OF RESULTS

III.A. Analysis and Results: Continuous Wave Green Laser

For a set incident pump power of 970 ± 20 mW, the average cw TEM_{00} power output for a >1-hr time interval was found to be stable to within a ±0.038% relative uncertainty. Although a value this low was not anticipated (considering that the cavity was not controlled by a TEC), this agrees with research by other parties which reported cw stability of <2% or <1% for similar laser systems.[45] In cw operation, several of the transverse electromagnetic modes were obtained. Photographs of the experimental transverse intensity profiles for these modes are displayed in Figure 8 alongside theoretical predictions.

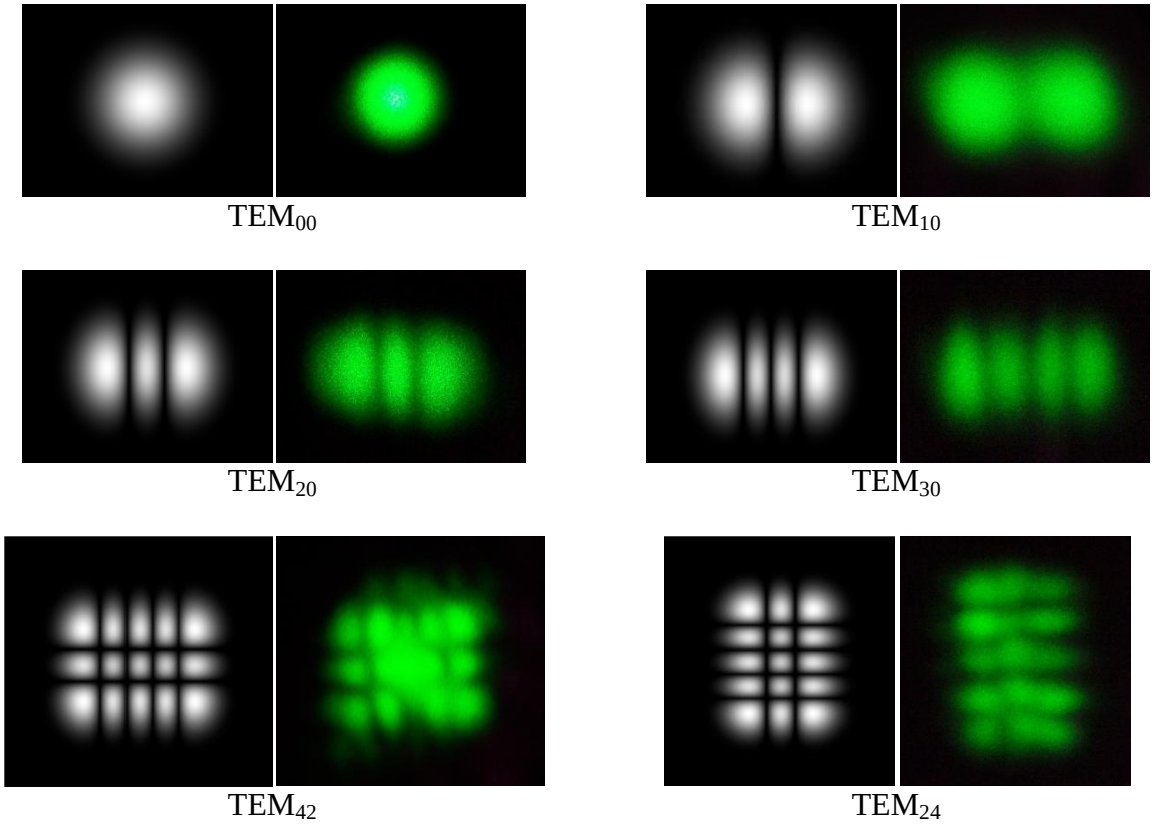

Figure 8: Transverse mode patterns for several *x*-*y* symmetries. (Left) Theoretical TEM_{pq} mode patterns.[46] (Right) Experimental TEM_{pq} mode patterns for cw laser.

III.B. Analysis and Results: Pulsed Green Laser

The most significant result of this experiment is that passive *Q*-switching with the Cr:YAG crystal could not be achieved; in fact, as long as it was present inside the cavity, the Cr:YAG prevented laser emission. The simplest and most logical explanation for this issue is that insufficient 1064 nm intensity was available to saturate the Cr:YAG crystal; recall that until the saturation intensity for such a crystal is reached, it absorbs the laser radiation. This implies that the pumping efficiency (the ratio of the amount of pumping energy converted into laser emission to the total available pumping energy) was very low. The fiber-coupled laser diode had a 16° cone-angle of divergence and thus because the two lenses utilized did not adequately collimate the pump beam, much of the divergent pump light was not directed into the Nd:YVO_4

crystal and was therefore wasted energy. Figure 9, a photograph of the cw laser illustrating the 'leaked' pump beam, corroborates this claim.

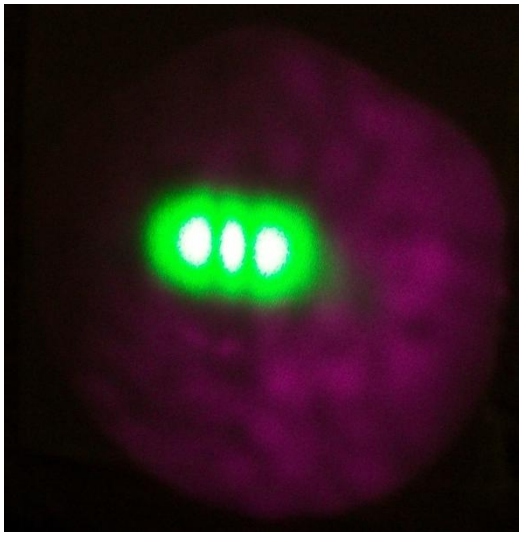

Figure 9: An oversaturated digital image of the cw laser in TEM_{20} operation projected onto a wall. The oversaturation allows the infrared radiation to be detected. The highly-divergent pump beam, apertured by the output coupler, can be seen as a reddish-purple hue. This provides qualitative evidence of poor pumping efficiency and therefore a reason that the Cr:YAG passive *Q*-switch could not be saturated.

Recall that active *Q*-switching by mechanical means is a viable alternative to the passive saturable absorber method. A pulsed laser was therefore obtained by replacing the Cr:YAG *Q*-switch element with a high-speed optical chopper.[47] Calibrated measurements of the average output power and peak power for the pulsed laser could not be made with the PIN photodiode, since the 808 nm and 1064 nm signals could not be separated from the 532 nm beam. In the future, the addition of an etalon to select the 532 nm light would facilitate this measurement. Instead of directly measuring the peak power, the ratio of the peak power to the cw power was calculated in order to continue analysis of the laser. The threshold at which the mechanically *Q*-switched 532 nm laser produced measurable pulses was 564.0 ± 2.0 mW for a chopper frequency of 3.921 ± 0.020 kHz. For a pulse width of 477 ± 32 ns (the shortest obtained in the experiment),

the pulsed laser was shown to have a peak-power-to-cw-power ratio of 12.28 ± 0.50 at a set incident pump power of 602 ± 2 mW.

Figure 10 shows the waveform for a single 532 nm *Q*-switched pulse as well as a series of laser pulses. The dependence of output power, pulse width, and pulse energy on incident pump power is illustrated in Figures 11-13, respectively. By comparing Figures 11 and 12, it can be seen that the shorter pulse widths correspond to higher peak-to-cw power ratios, which is consistent with theoretical predictions for *Q*-switched pulses given above. Another straightforward expected result is confirmed in Figure 13: as more pumping energy is used, the energy per pulse in the output increases for a set repetition rate.[48] The nonlinear increasing trend in this plot at low pump powers is related to the very narrow width of the pulses; in fact, the relationships between pulse width and pulse energy appears linear (see Figure 14). Intriguingly, the peak-cw power ratio decreases and the pulse width increases with increasing pump power, as seen in Figures 12 and 13 (and as summarized in Figure 14). Literature shows that for both electro-optically *Q*-switched and double *Q*-switched Nd:YVO_4 and Nd:YVO_4/KTP systems, these trends should be increasing and decreasing, respectively.[49] This however, is slightly misleading, since in the published systems, the peak pulses were absolutely measured. In this experiment the peak power was measured relative to the cw power, which was not fixed, but rather increased with pump power as well. This is further reasoning to support the filtering of the output light to obtain calibrated power readings. The puzzling result that remains is the increasing pulse width trend;

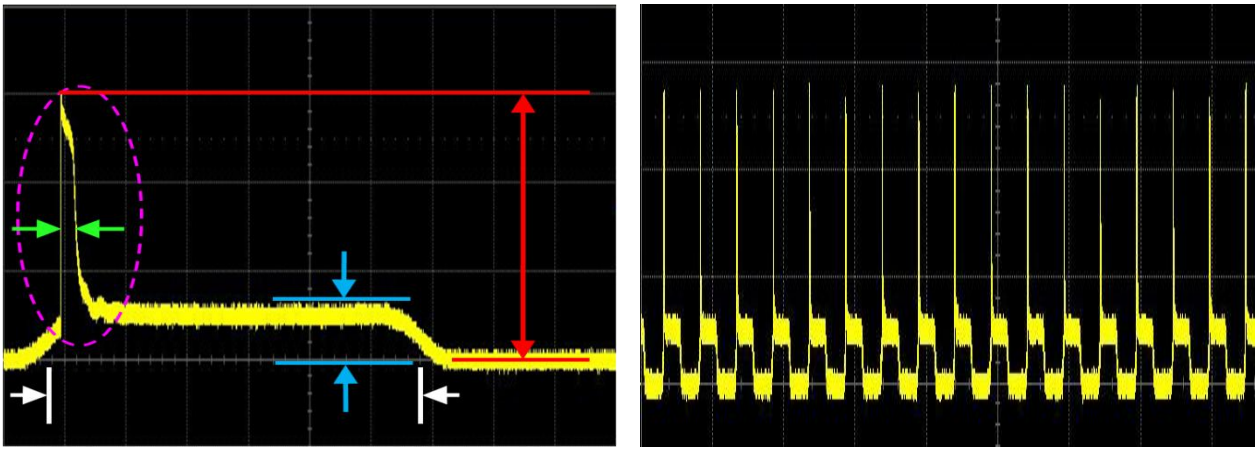

Figure 10: (Left) The waveform for a single 532 nm mechanically *Q*-switched pulse. The duration for which the beam is unblocked by the optical chopper is designated by the white dimension, the green arrows denote the pulse width (FWHM), the blue dimension indicates the cw power, the red dimension indicates the peak power of the pulse, and the dashed magenta line indicates the portion of the waveform for which the pulse energy was determined (the area under the waveform with the max cw power as the baseline). The ratio of the peak power to cw power was calculated as the ratio of the magnitude of the dimension in red to the magnitude of the dimension in blue. (Right) A waveform demonstrating the temporal distribution of multiple *Q*-switched pulses.

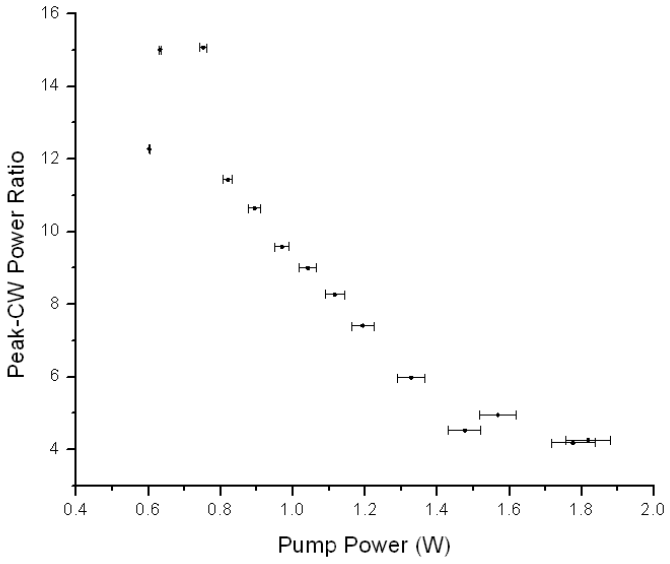

Figure 11: The ratio of peak power to cw power as a function of pump power for LD-pumped 532 nm passively *Q*-switched Nd:YVO_4 laser.

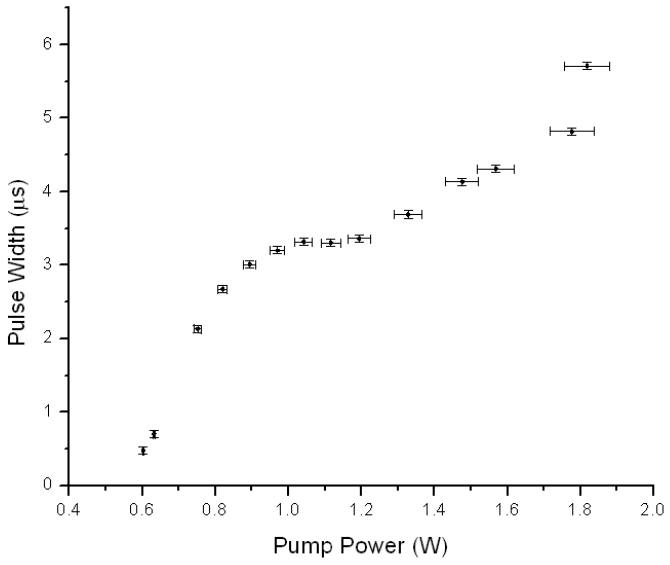

Figure 12: Pulse width vs. pump power for LD-pumped 532 nm passively *Q*-switched Nd:YVO_4 laser.

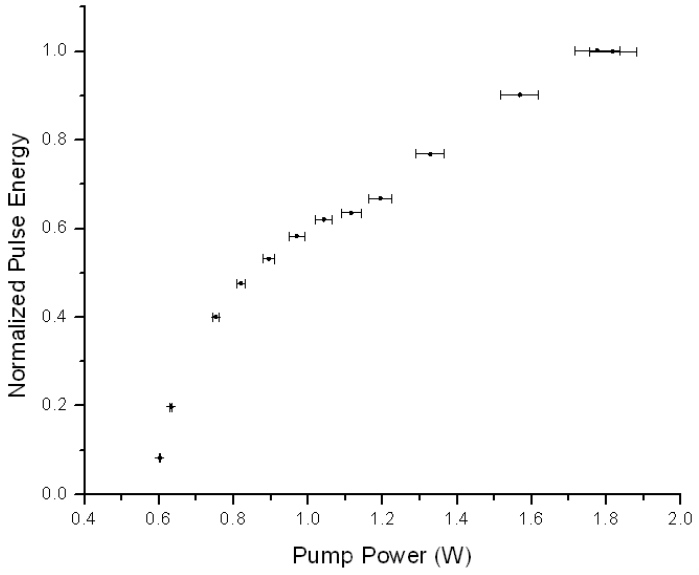

Figure 13: Normalized pulse energy as a function of pump power for LD-pumped 532 nm passively *Q*-switched Nd:YVO_4 laser.

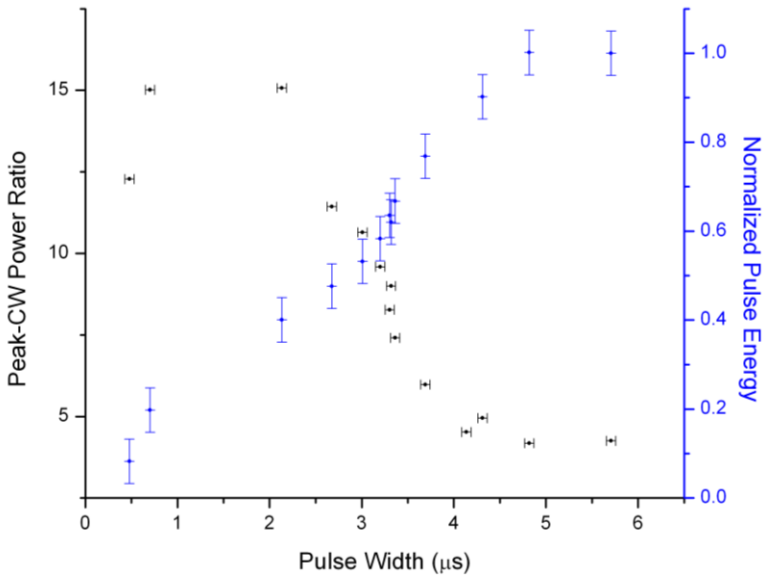

Figure 14: Peak-power-to-cw-power ratio (black) and normalized pulse energy (blue) vs. pulse width for LD-pumped 532 nm passively *Q*-switched Nd:YVO_4 laser.

IV. SUMMARY AND CONCLUSION

A diode-pumped 532 nm Nd:YVO_4 laser with active *Q*-switching and intracavity KTP frequency doubling was constructed. The shortest pulse width achieved in this experiment was 477 ± 32 ns, which had a corresponding peak-power-to-cw-power ratio of 12.28 ± 0.50; this is a sufficiently short pulse for this laser to be suitable for interferometric or holographic applications, which was a goal for this project. Additional work is proposed to modify the pump-cavity coupling mechanism such that the pumping efficiency can be improved, the Cr:YAG crystal ultimately being used as a working passive *Q*-switch. The Cr:YAG offers a more compact and cost-effective solution, and offers better performance (higher repetition rate, shorter pulse widths, and higher pulse energy). The implementation of an etalon is suggested as a means of forcing single-frequency operation and facilitating the accurate measurement of the laser's capabilities.

ACKNOWLEDGEMENTS

This work was supported by the University of Wisconsin-River Falls Physics Department. The author thanks Dr. Lowell McCann (Univ. of Wisconsin-River Falls, Dept. of Physics) for his mentorship on the project.

---

[1] Fan, T. Y., IEEE J. Quantum Electron. **27** (9), 2091-2093 (1991); Nagai H. *et al*., IEEE J. Quantum Electron. **28** (4), 1164-1168 (1992); Chee, J. K. and Choi, B. S., Opt. Commun. **118**, 289-296 (1995); Clarkson, W. A. and Hanna, D. C., Opt. Lett. **21** (12), 869-871 (1996); Martin, K. I., Clarkson, W. A., and Hanna, D. C., Opt. Lett. **21** (12), 875-877 (1996); Yelland, C. and Sibbett, W., J. Mod. Opt. **43** (5), 893-901 (1996); Chen, Y.-F., *et al*., Appl. Opt. **37** (24), 5727-5730 (1998); Shen, D. and Ueda, K., Opt. Rev. **5** (6), 363-368 (1998); Shen, D., *et al*., Appl. Opt. **37** (33), 7785-7788 (1998); Zhdanov, B. Z., Andersen, G. P., and Knize, R. J., Am. J. Phys. **68** (3), 282-286 (2000); Friel, G. J., *et al*., Appl. Opt. **39** (24), 4333-4337 (2000).
[2] Zheng, Q., *et al*., Opt. Laser Technol. **34**, 425-427 (2002); Taira, T. and Kobayashi, T., Appl. Opt. **34** (21), 4298-4300 (1995); Zheng, Q. and Zhao, L., Opt. Laser. Technol. **34**, 239-241 (2002).
[3] Zheng, *et al*. op. cit., 425; Zheng, op. cit., 239.
[4] W. T. Silfvast, *Laser Fundamentals* (Cambridge University Press, New York, 2004), 199-202.
[5] *Ibid*. p. 216.
[6] *Ibid*. p. 218-219.
[7] *Ibid*.
[8] Figure: *Ibid*. p. 217.
[9] *Ibid*. p. 216.
[10] *Ibid*. p. 229-234, p. 245-246.
[11] *Ibid*. p. 235-245.
[12] *Ibid*. p. 247-249.
[13] *Ibid*. p. 371-373.
[14] *Ibid*. p. 381.
[15] *Ibid*. (figure based on Figure 11-7 on p. 383).
[16] *Ibid*. p. 379-383.
[17] *Ibid*. p. 386.
[18] *Ibid*. p. 386-387, p. 392-392.
[19] Figure adaptation: *Ibid*. p. 386.
[20] H. Margenau and G. M. Murphy, *The Mathematics of Physics and Chemistry* (D. Van Nostrand Company, Inc., Princeton, 1956), 246-254.
[21] Op. cit. 4, p. 388-389.
[22] Op. cit. 20, p. 358-360; op. cit. 19, p. 121-126.
[23] *Ibid*. p. 123.
[24] Op. cit. 4, p. 601-615 (for more information on frequency multiplication and nonlinear optical effects).
[25] *Ibid*. p. 610-615.
[26] *Ibid*. p. 446-449.
[27] *Ibid*. p. 449-450.
[28] Op. cit. Zheng *et al*., p. 425-426.
[29] Shen and Ueda, op. cit., 366; Zheng, *et al*. op. cit., 426; Zheng, op. cit., 239.
[30] HR: P/N DPO0402 (Casix, Inc., Fuzhou, Fujian 350014, China).
[31] OC: P/N DPO0301-200 (Casix, Inc., Fuzhou, Fujian 350014, China).
[32] LD: GaAlAs semiconductor laser, P/N SFA100-808-R1-01 with SMA-905 connector (Newport Corporation, Spectra-Physics Laser Division, Santa Clara, CA, 95054) was used in conjunction with a fiber-coupled single emitter (Opto Power Corporation, Tucson, AZ, 85706). A +5V laser diode driver (Model PLDPCB-5000, S/N 00F017268) was used to control the LD (Wavelength Electronics, Inc., Bozeman, MT, 59771).
[33] TEC was a Thermoelectric & Resistive Heater Temperature Controller, Model PID-1500, S/N 00B017267 (Wavelength Electronics, Inc., Bozeman, MT, 59771).

[34] The lens (P/N KPX 076AR.16) used to focus the pump beam into the Nd:YVO_4 crystal was plano-convex and AR-coated for 650-1000 nm (Newport Corporation, Irvine, CA, 92606).
[35] Nd:YVO_4: P/N DPO3101, Fabrication No. B08063 (Casix, Inc., Fuzhou, Fujian 350014, China).
[36] KTP: P/N DPO6101, Fabrication No. B08064 (Casix, Inc., Fuzhou, Fujian 350014, China).
[37] The Cr:YAG crystal had P/N DP07205-85% and Casix Item# 30120493 (Casix, Inc., Fuzhou, Fujian 350014, China).
[38] Alignment laser: 17.0 mW HeNe laser, Model LHRP-1701, S/N 6083-0900-1701 (Research Electro-Optics, Inc., Boulder, CO, 80301).
[39] The HR and OC mirrors were mounted in Newport Model HVM-.5 vertical-drive kinematic optical mounts (Newport Corporation, Irvine, CA, 92606).
[40] The mounts to which the copper blocks containing the Nd:YVO_4 and KTP crystals were attached were Newport Model GM-1R precision rotation mounts (Newport Corporation, Irvine, CA, 92606).
[41] The mount to which the copper block holding the Cr:YAG crystal was attached was a Newport Model RSP-1T rotation stage with coarse and fine adjustment capabilities (Newport Corporation, Irvine, CA, 92606).
[42] Continuous wave power was measured with a Newport Power Meter (Model 1815-C, S/N 4208) attached to an OD3 attenuator (Model 883-SL, S/N 9253) (Newport Corporation, Irvine, CA, 92606).
[43] A LeCroy WaveSurfer 44Xs digital oscilloscope (S/N LCRY0304M11612) was used for cw avg. power and stability measurements, as well as pulsed operation characterization (LeCroy Corporation, Chestnut Ridge, NY, 10977).
[44] PIN photodiode: P/N OSD15-5T, Lot # Y7869 (Thermo Centrovision, Inc., Newbury Park, CA, 91320). The photodiode data collection method was adapted from the Photoconductive Bias Mode outlined in the following document: <http://www.osioptoelectronics.com/application-notes/AN-Photodiode-Parameters-Characteristics.pdf> (OSI Optoelectronics, Inc., Hawthorne, CA, 90250).
[45] Op. cit. Shen, *et al*., p. 7787; op. cit. Shen, p. 366; op. cit. Chee and Choi, p. 295; op. cit. Chen, *et al*. p. 5729.
[46] Images adapted from "Hermite-gaussian.png" obtained Web 19 December 2009, <http://en.wikipedia.org/wiki/File:Hermite-gaussian.png>. Edited according to theory: Op. cit. 4, p. 389.
[47] New Focus Optical Chopper (Model 3501) with 42/30 slot wheel accessory (Model 3513) (Newport Corporation, Irvine, CA, 92606).
[48] Wang, *et al*., Opt. Eng. **46** (5), 054202-5 (2007).
[49] Op. cit. 48, p. 054203, 054206; op. cit.

APPENDIX A. LASER OPERATING PROCEDURE

Table 1 presents a step-by-step start-up and shut-down procedure for operating the laser.

Start-up Procedure	
1	Connect a digital multimeter (DMM) to the 'Monitor +' and 'Monitor -' terminals on the LD's PID temperature controller (TEC). Turn the 'Monitor Select' switch to 'Set T.' Ensure that the 'Output Enable' switch is in the 'off' position.
2	Turn on the power switch for the TEC. Using a small screwdriver, adjust the set-point temperature ('Temp Set') to 27°C (about 1.55V).
3	Connect a second DMM to the 'Monitor +' and 'Monitor –' terminals on the LD driver. Ensure that the 'Monitor Select' switch is set to 'Monitor I' in order to monitor the input current to the LD. Ensure that the 'Laser Disable' switch is selected. Turn on the power switch for the LD driver.
4	Turn on the 'Output Enable' switch for the TEC.
5	Using a small screwdriver, set the LD input current to be just above the threshold for stimulated emission (about 0.26 V on I monitor).
6	Switch the LD driver to 'Laser Enable.'
7	Gradually increase the current to obtain the desired pump power.
Shut-down Procedure	
1	Lower the LD current to below the threshold for stimulated emission.
2	Switch the LD driver to 'Laser Disable' and the TEC to 'Output Disable.'
3	Turn off the power switches for the LD driver and TEC. Turn off the DMMs.

Table 1: Start-up and shut-down procedure for the laser.